

Self-Powered Gesture Recognition Wristband Enabled by Machine Learning for Full Keyboard and Multicommand Input

Puchuan Tan, Xi Han, Yang Zou, Xuecheng Qu, Jiangtao Xue, Tong Li, Yiqian Wang, Ruizeng Luo, Xi Cui, Yuan Xi, Le Wu, Bo Xue, Dan Luo, Yubo Fan,* Xun Chen,* Zhou Li,* and Zhong Lin Wang

Virtual reality is a brand-new technology that can be applied extensively. To realize virtual reality, certain types of human–computer interaction equipment are necessary. Existing virtual reality technologies often rely on cameras, data gloves, game pads, and other equipment. These equipment are either bulky, inconvenient to carry and use, or expensive to popularize. Therefore, the development of a convenient and low-cost high-precision human–computer interaction device can contribute positively to the development of virtual reality technology. In this study, a gesture recognition wristband that can realize a full keyboard and multicommand input is developed. The wristband is convenient to wear, low in cost, and does not affect other daily operations of the hand. This wristband is based on physiological anatomy as well as aided by active sensor and machine learning technology; it can achieve a maximum accuracy of 92.6% in recognizing 26 letters. This wristband offers broad application prospects in the fields of gesture command recognition, assistive devices for the disabled, and wearable electronics.

1. Introduction

Virtual reality provides users with an immersive experience by simulating specific scenes in reality and has been widely used in education, medical care, military, industrial production, and other fields.^[1] To realize virtual reality, users must be provided with various sensory stimuli to simulate real scenes. Meanwhile, the virtual reality system must obtain the user's location information, real-time action information, physiological signals, and command information issued by the user.^[2–4] Therefore, the design of various types of human–computer interaction (HCI) devices is particularly important for the development of virtual reality.^[5–7] The hand is the most flexible organ of

P. Tan, Y. Xi, Y. Fan
Beijing Advanced Innovation Centre for Biomedical Engineering
Key Laboratory for Biomechanics and Mechanobiology of Ministry of Education
School of Biological Science and Medical Engineering
Beihang University
Beijing 100191, P. R. China
E-mail: yubofan@buaa.edu.cn

P. Tan, X. Han, Y. Zou, X. Qu, J. Xue, T. Li, Y. Wang, R. Luo, X. Cui,
Y. Xi, D. Luo, Z. Li, Z. L. Wang
CAS Center for Excellence in Nanoscience
Beijing Key Laboratory of Micro-nano Energy and Sensor Beijing
Institute of Nanoenergy and Nanosystems, Chinese Academy of Sciences
Beijing 101400, P. R. China
E-mail: zli@binn.cas.cn

X. Han, T. Li, Y. Wang, R. Luo, Z. Li
Center on Nanoenergy Research
School of Physical Science and Technology
Guangxi University
Nanning 530004, P. R. China

Y. Zou, J. Xue
School of Life Science
Institute of Engineering Medicine
Beijing Institute of Technology
Beijing 100081, P. R. China
X. Qu, X. Cui, Z. Li, Z. L. Wang
School of Nanoscience and Technology
University of Chinese Academy of Sciences
Beijing 100049, P. R. China

L. Wu, B. Xue, X. Chen
Department of Electronic Engineering and Information Science
University of Science and Technology of China
Hefei, Anhui 230026, P. R. China
E-mail: xunchen@ustc.edu.cn

Z. Li
Institute for Stem Cell and Regeneration
Chinese Academy of Sciences
Beijing 100101, P. R. China

Z. L. Wang
School of Materials Science and Engineering
Georgia Institute of Technology
Atlanta, GA 30332, USA

 The ORCID identification number(s) for the author(s) of this article can be found under <https://doi.org/10.1002/adma.202200793>.

DOI: 10.1002/adma.202200793

the human body. The human hands can perform various rapid gestures. Using gestures as the input method in HCI provides a new solution and research direction for realizing virtual reality.^[8]

Cameras, mechanical sensors, and electromyography (EMG) sensors are typically used to acquire movement information in existing gesture recognition technologies (Table S1, Supporting Information).^[9–11] Combined with these three technologies, the current gesture recognition devices can realize a real-time gesture recognition function.^[12] Gesture recognition devices based on image recognition technology must be equipped with a high-precision camera when in use. Gesture recognition devices based on mechanical sensors offer a wide range of sensor options, such as triboelectric, piezoelectric, piezoresistive, and capacitive sensors.^[13,14] Most of these devices are attached to the user's finger knuckles or are directly formed into gloves to acquire mechanical data. Because surface EMG signals are difficult to detect and always overwhelmed in noise, signal processing and extraction are vital to gesture recognition devices that use EMG sensors. Usually, two or more of the sensors above are used to gather data at the same time to improve the accuracy of gesture recognition.

Human hand movements are extremely complicated, and simple hand movements often involve almost all the muscle groups of the hand.^[15,16] Some of these muscle groups are near the surface of the skin, including the extensor digitorum, extensor digiti minimi, flexor digitorum superficialis, extensor carpi ulnaris, and so on, which are crucial for performing a gesture. Most of the muscle belly or tendon passes through the wrist. Therefore, a wristband-style mechanical device with multiple sensors can be placed on the wrist to acquire mechanical information from muscles near the skin's surface; as such, the hand movement can be inferred, and specific gestures can be recognized.^[15]

This wristband-style mechanical device is easy to wear, does not affect the user's other tasks, and significantly improves user experience.^[17] The wristband-style mechanical device can obtain all mechanical information from the surface muscles of the hand. However, in most conditions, the action from one finger often triggers multiple sensors on the wristband, unlike the case when sensors are attached to the user's finger knuckles. Therefore, gestures generate diverse signals in multiple sensor channels. If signals from different sensors can be decoded, then all gestures can be revealed using a wristband-style device. In this regard, data processing and analysis are crucial, and more advanced data processing methods are necessitated. Using a few basic signal processing methods combined with the machine-learning algorithm of the linear discriminant analysis (LDA) model, diverse mechanical information obtained from multiple sensors can be fully utilized to improve recognition accuracy.^[18–20]

A gesture recognition wristband (GRW) enabled by machine-learning technology was developed. Using two types of devices as active sensors, triboelectric nanogenerators (TENGs) and piezoelectric nanogenerators (PENGs), the GRW can obtain mechanical information regarding hand movement precisely without consuming electricity. Combined with the machine-learning algorithm of the LDA model, the GRW achieved letter-by-letter recognition of sign language actions, with a

maximum recognition accuracy of 92.6%. Additionally, this wristband can be used as a typing input device for real-time voice broadcasting.

2. Results and Discussion

A machine-learning-based smart wristband system that can recognize sign language, translate it in real time, and broadcast the wearer's sign language actions via voice was developed (Figure 1a). The entire system completes tasks such as data acquisition, processing, and analysis. Specifically, the system includes a smart wristband, an eight-channel Bluetooth module, and a mobile computer terminal (Figure S1a, Supporting Information). A sensor array and a flexible printed circuit board (FPCB) are included in the wristband, and each sensor array contains eight sensors (Figure 1b). Figure 1c depicts a single sensor based on a hybrid generator consisting of a TENG and a PENG. Each sensor comprised a polydimethylsiloxane (PDMS) layer (thickness of 2 mm), polylactic acid (PLA) frame (length: 10 mm; width: 8 mm; height: 4 mm), a polyvinylidene fluoride (PVDF) layer (thickness of 0.1 mm), a copper layer (thickness of 0.3 mm), two layers of FPCB (thickness of 0.1 mm), and a rectifier bridge. The eight sensors were connected by two layers of the FPCB (length of 18 cm). The two layers of the FPCB serve as the wristband's connection structure and the circuit carrier of the entire array (Figure 1d). As a communication interface with the eight-channel Bluetooth module, two sets of pins are created from the end of the FPCB. Owing to the large internal resistance of the hybrid generator, an effective circuit design is required to achieve impedance matching before the signal is transmitted to the sensor (Figure S2, Supporting Information).

As shown in Figure S1c in the Supporting Information, the overall goal of the system is to convert and analyze different types of signals. The sensor obtains mechanical information from the wrist and converts it into electrical information, whereas the Bluetooth module wirelessly transmits the electrical information obtained to the computer. Subsequently, the electrical information is processed using a computer. Butterworth low-pass filtering, baseline repair, independent component analysis (ICA), and feature extraction are among the processing techniques used. Finally, a mathematical model was built based on the extracted features and the LDA method (Figure 1e,f). This model is used to complete the recognition task of sign language actions.

A mechanical sensor array based on a hybrid generator was designed to obtain hand movement information in various motion states. Each sensor included a TENG and a PENG. The TENG and PENG were primarily used to obtain mechanical information regarding motions with large force and slight contact, respectively.^[14,21–23] Figure 2a shows the power-generation principle of the PENG. Consider the first action as an example. The circumference of the wrist increases with the wrist muscles contraction. Because the wristband's circumference is fixed, the muscles and skin exert pressure on the contact surface of the sensor. The piezoelectric film deforms and generates an induced electric potential. The piezoelectric film undergoes a series of deformation over a movement cycle, as follows: no deformation, slight deformation, maximum deformation, slight

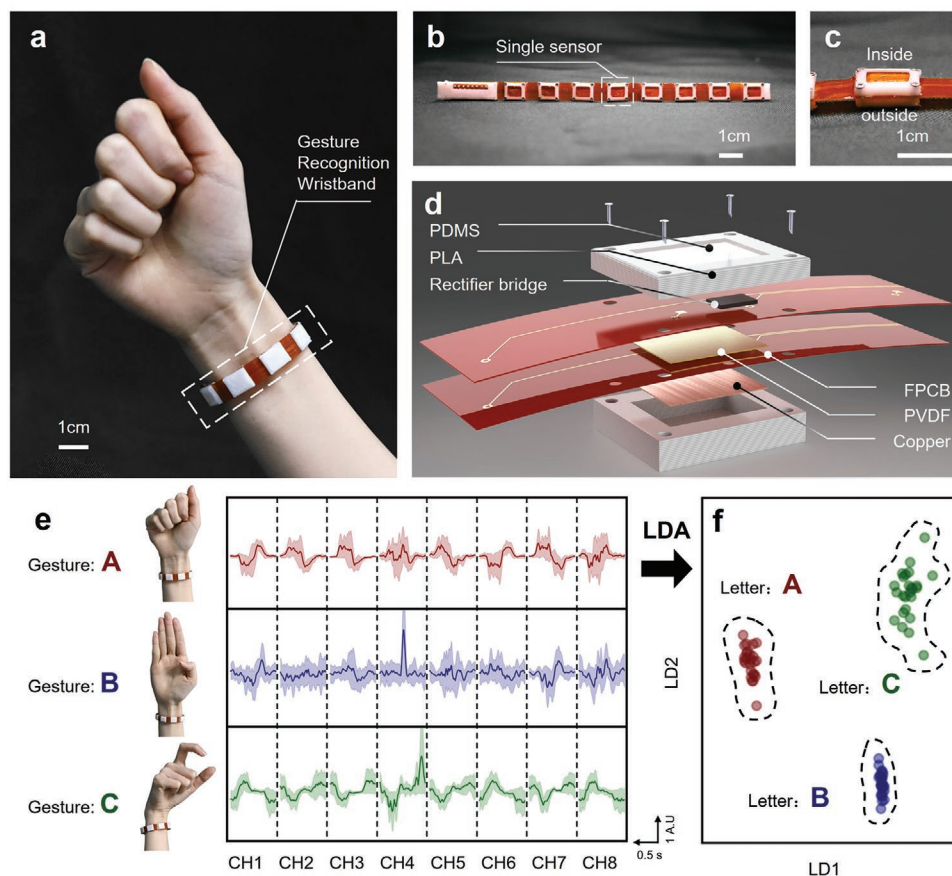


Figure 1. Overview of GRW system: a) Photograph of GRW. b) Schematic diagram of GRW's sensor array. Each sensor array contains eight sensors. c) Schematic diagram of single sensor. d) Schematic diagram of single sensor of GRW, where materials used are shown. e, f) Processing procedure from sign language database to machine-learning model based on LDA.

deformation, and no deformation. Similarly, the induced potential changes regularly, resulting in an alternating current. The power generation mechanism of the TENG is based on changes in the contact area and the distance between the skin and PDMS layer on the sensor surface; as such, mechanical information produced by motion with slight contact can be obtained easily. Using hand shaking as an example, the device surface and skin surface will be in repeated contact and separation when the hand is repeatedly rocked over by the movement of the wrist joints. Because the skin and PDMS attract charges differently, they will possess different types of charges and form different charge centers. The sensing layer inside the PDMS generates a periodic alternating current because the distance between the centers of the two types of charge changes regularly. Using COMSOL Multiphysics, we conducted a simulation study pertaining to the force-deformation and electric potential of a single sensor to better understand the device's power generation principle, and the results are consistent with the actual results (Figure 2b,c). Furthermore, we compared the mechanical information collection capabilities of the two types of generators used in the device for different motion states. As shown in Figure 2d, the output of the TENG of the hybrid generator was higher when the hand shaking motion (which corresponds to the motions with slight contact) was completed, whereas the PENG contributed yielded a higher output when fist motions

were performed (Figure 2e, which corresponds to the motions with large force).

To further elucidate how the signals of TENG and PENG are superimposed, we compared the difference in voltage amplitude between using TENG alone as a sensor, using PENG alone as a sensor, and using a hybrid generator as a sensor, respectively. The hybrid generator not only improves the amplitude of the voltage, but also retains some details of the PENG and TENG signals, which provides more useful information for later feature engineering (Figure S3a, Supporting Information). Meanwhile, we compare the signal of the hybrid generator with the arithmetic sum of the signal of PENG and TENG. As shown in Figure S3b in the Supporting Information, the signal of the hybrid generator has a relatively high coincidence with the arithmetic sum of the signal of PENG and TENG, both in amplitude and shape.

An anatomical illustration of the superficial muscle groups involved in wrist movement is presented (Figure 3a). The locations of the sensors are indicated. Using this diagram, the effects of various gesture movements on specific sensors can be assessed promptly based on the muscles involved in different finger movements. The sensor designed based on the hybrid generator is essentially a mechanical sensor; therefore, we performed a force–voltage calibration on the sensor. As shown in Figure S4a in the Supporting Information, the single sensor

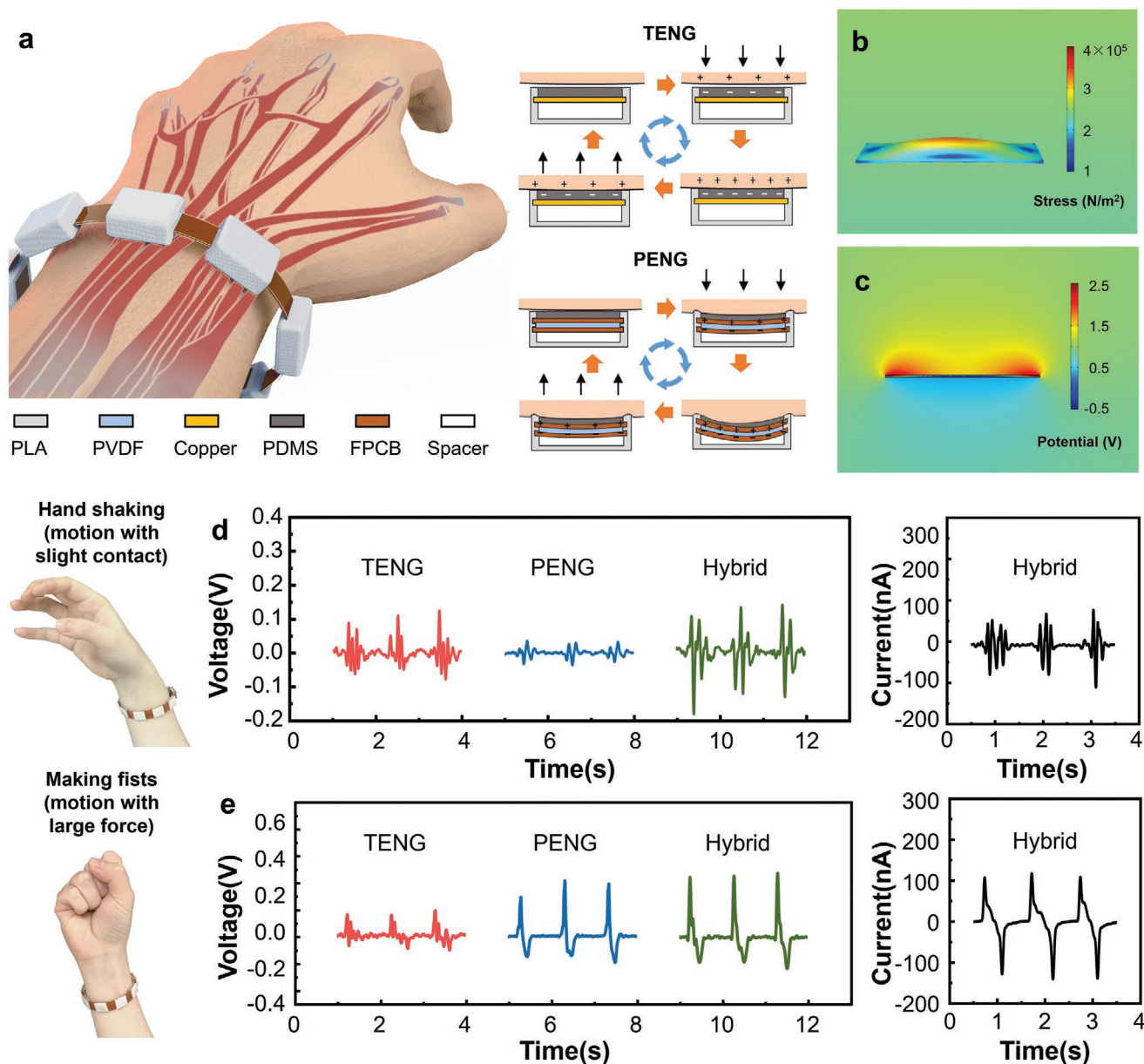


Figure 2. Operating principle of hybrid generator in GRW: a) Operating principle of PENG and TENG in GRW. The sensor is close to tendons (the dark red long object in figure) under the skin. b) Stress and c) potential on PDMS surface when hand is performing a gesture. d) Voltage and current signal of single sensor during hand shaking, which corresponds to motions with slight contact; in this case, TENG provides more contribution. e) Voltage and current of single sensor during making fists, which corresponds to motions with large force; in this case, contribution from PENG is higher. Hybrid generator exhibits higher voltage amplitude in both two motions.

exhibited good linearity when the force was within 7 N, and this range encompassed the range of the force applied by the wristband to the wrist skin. Next, we compared the proposed sensor with a standard commercial mechanical sensor. It was observed that the output of the proposed sensor was higher than that of a commercial mechanical sensor under the same mechanical load (Figure S4b, Supporting Information). Because wearable devices must be worn for lengthy durations and require high mechanical stability, we performed more than 5000 fatigue tests on this wristband. At the beginning, intermediate, and final stages, the device maintained a stable output of ≈ 30 mV, as

shown in Figure S4c in the Supporting Information. Due to the different wearers and the randomness of wearing, the wearing angle and tightness may be different, which will have a greater impact on the voltage output results. Therefore, we explored the voltage output change when the GRW was at different angles (Figure 3b) and when the GRW was worn by people of different body types (Figure 3c). From the figure, we can observe that after the position of a single sensor changes, the voltage output change is very small, but a small displacement change in some important positions will cause a sudden change in the voltage output of the sensor (e.g., when the angle of the No. 1 sensor

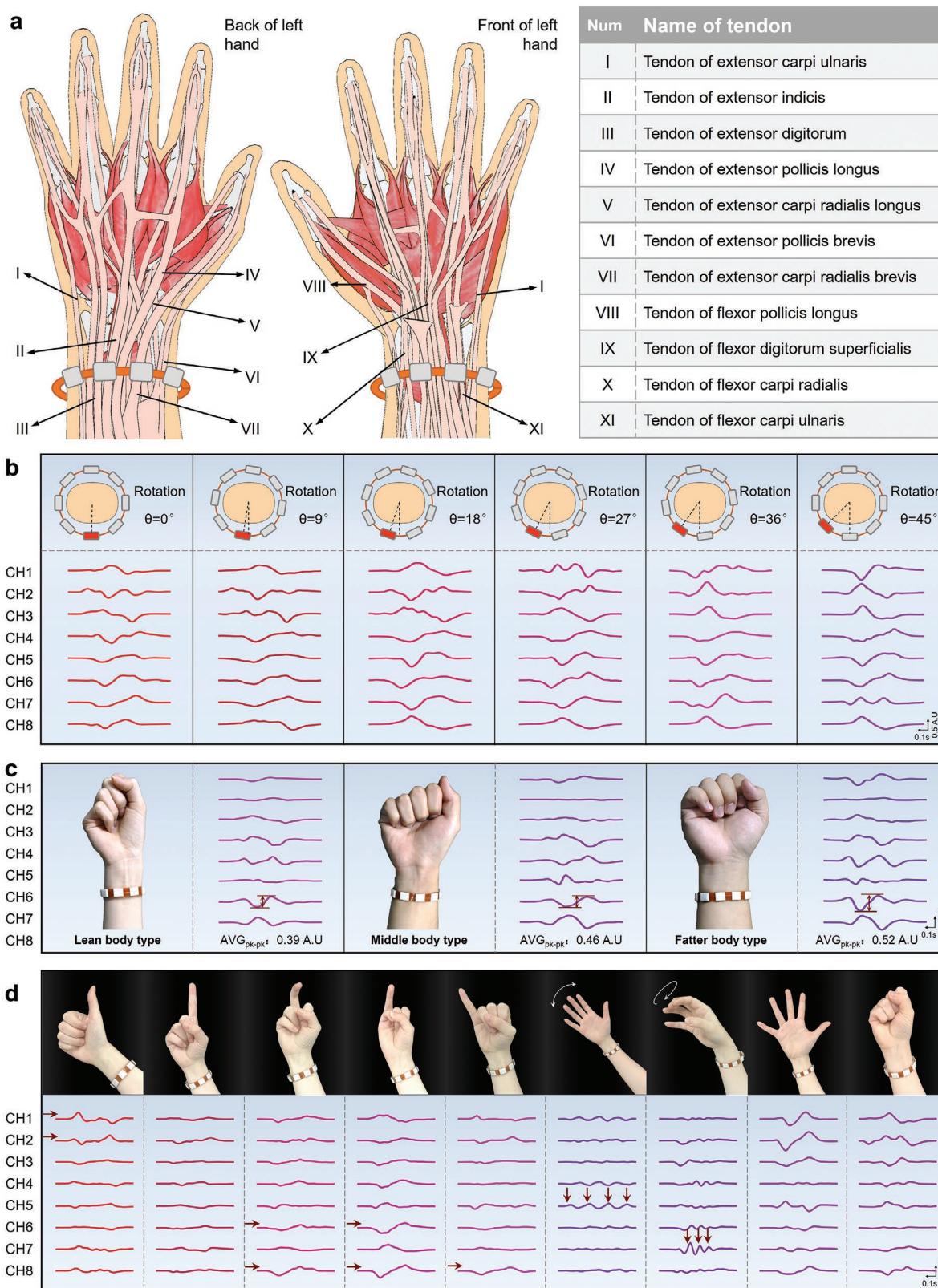


Figure 3. Electrical performance of GRW and sensor signal of specific gestures: a) Sensor position and anatomy of hand muscles. b) Comparison of output changes when GRW is at different angles. From left to right, angles between GRW and initial position are 0° , 9° , 18° , 27° , and 45° . c) Comparison of output changes when GRW is worn by people of different body types. d) Sensor signal of some specific gestures. Individual extensions of five fingers, as well as specific hand motions such as arm swing, hand shaking, hand opening, and fist making are presented.

is from 18° to 36°, the waveform of the sensor changes greatly. At this time, the position of the No. 1 sensor leaves the tendon sheath of the flexor pollicis longus and crosses the scaphoid). And the voltage output of the GRW increased when it was worn by a person with a wider body. This kind of difference between people and the randomness of wearing is an objective existence, and it is difficult to avoid this problem in the design of the device. The introduction of machine learning can effectively solve this problem. When the wearing conditions change, the GRW can re-learn the wearer's gestures, and after the learning is complete, it can recognize the types of gestures under the new conditions. Finally, as shown in Figure 3d, we used the sensor array to obtain information regarding several fundamental wrist movements, such as the movement of a single finger (thumb to little finger) and other pre-set typical actions (swing arm, hand shaking, opening hand, fist). The effects of various movements on the output of the sensor array as well as those of the significant difference were readily visible. For example, the movement of the thumb primarily affected sensors No. 1 and No. 2, and these two sensors were located at the base of the thumb. In another example, both arm swing and hand shaking exhibited significant periodic fluctuations, however, hand shaking exhibited a higher frequency but a lower output. These results are consistent with the actual measurement results. To enable the readers to better understand the sign language gestures used, a description of letters and gestures is tabulated in Figure S5 in the Supporting Information.

The system employs a few data processing methods to calculate the features of each action electrical signal and create a feature matrix; subsequently, the latter is combined with the classification labels to develop an LDA classification model. The complete data processing and analysis procedure was classified into four procedures to construct a machine-learning model (Figure 4a). The first step was noise reduction. The original data were filtered using a Butterworth low-pass filter with a cut-off frequency of 20 Hz. The TENG exhibited baseline drift due to the accumulation of static electricity over time; in this regard, we performed a Fourier transform to intercept a signal of less than 1 Hz in the original data and then removed it to complete the baseline repair. The second step was fast ICA. The movement information of the five fingers was obtained using eight sensors; the signal obtained for each sensor was a mixed signal. Hence, we used the fast independent component analysis method to analyze those signals to obtain motion information for a single finger and increase the model's prediction accuracy. The third step involved feature engineering. Each piece of valid waveform data was subjected to feature extraction. The maximum value, minimum value, peak–valley interval, zero-crossing point numbers, inflection point numbers, and absolute square values were selected as feature values. Figure S6 in the Supporting Information depicts this procedure. Figure S7 in the Supporting Information illustrates the process by which different features function for the recognition of different letter pairs. To create an LDA prediction model, the feature matrix and gesture label were matched. Figure 4b shows a confusion matrix for 26 sign language gestures with different numbers of channels. Figure 4c shows the projection of 26 types of sign language gesture information on a 2D plane after processing was performed using different numbers of channels. When the

number of channels was eight, it was observed that the model effectively distinguished most gestures. The 26 types of sign language gestures exhibited a clear clustering tendency. The first type was a fist-like gesture resembling the letters M, E, O, S, and T, whereas the other was an open-hand-like gesture resembling the letters C, N, K, V, and Y (Figure S8, Supporting Information). The detailed data processing process is shown in Figure S9 in the Supporting Information. Figure 4d shows the change in the model accuracy as the sample size increases with the number of channels used. As the number of channels increased, the model precision improved. When the number of channels was eight, the prediction accuracy of the model no longer improved significantly (Figure S10, Supporting Information). The maximum overall prediction accuracy was 92.6%.

Sentences, not letters, are the basic units of communication in daily life. Hence, we utilized the wristband as a keyboard input device to recognize the user's real-time sign language motion, transform it into a sentence, and broadcast it via voice (Figure 5a). The participants of our experiment wore the wristband to perform a sign language action every 1 s and then relaxed for 1 s when no input was provided. After completing the sign language action for the entire sentence, the participants relaxed completely and waited until the computer finished calculating the results. Figure 5b,c shows the waveform data for each channel as well as the computer recognition process during sentence input. The computer detected letters and spaces individually, saved the input data, and then displayed them on the screen. When the computer detected three space characters successively, it displayed all of the cached sentences and then cleared the buffer, ready for the next input (Videos S1–S3, Supporting Information).

We developed an eight-channel sensor wristband that combines active sensors and machine-learning technologies to recognize sign language. To acquire more mechanical data, a hybrid generator composed of a TENG and PENG was incorporated in the wristband. The output of the hybrid generator was ≈ 80 mV when the force applied by the wearer's skin to the sensor was 5 N. The hybrid generator design enables the wristband to obtain mechanical data from both motions with slight contact and large force simultaneously, thereby enriching the mechanical data obtained and increasing recognition accuracy. For machine learning, we used the LDA model. The participant wore the wristband and trained the recognition model for 26-letter gestures. The maximum prediction accuracy of the model for each gesture was 92.6% after 600 iterations of repeated training. We used this smart wristband system for sign language translation, which can realize the real-time broadcast of the word “Nano biolab.” Additionally, we used the GRW to complete the signal acquisition of numbers 0–9 and some specific gestures. Based on these data, the GRW can function as a full keyboard input device that can be used as an HCI device to provide data input for virtual reality applications.

In this study, we developed a sophisticated, highly integrated, and real-time GRW that can be utilized as a terminal for HCI in gesture recognition, mechanical control, keyboard input, and other scenarios.^[24] Mobile HCI terminals have recently garnered considerable attention and used in several studies.^[25–27] However, issues pertaining to the development of HCI terminals remain.

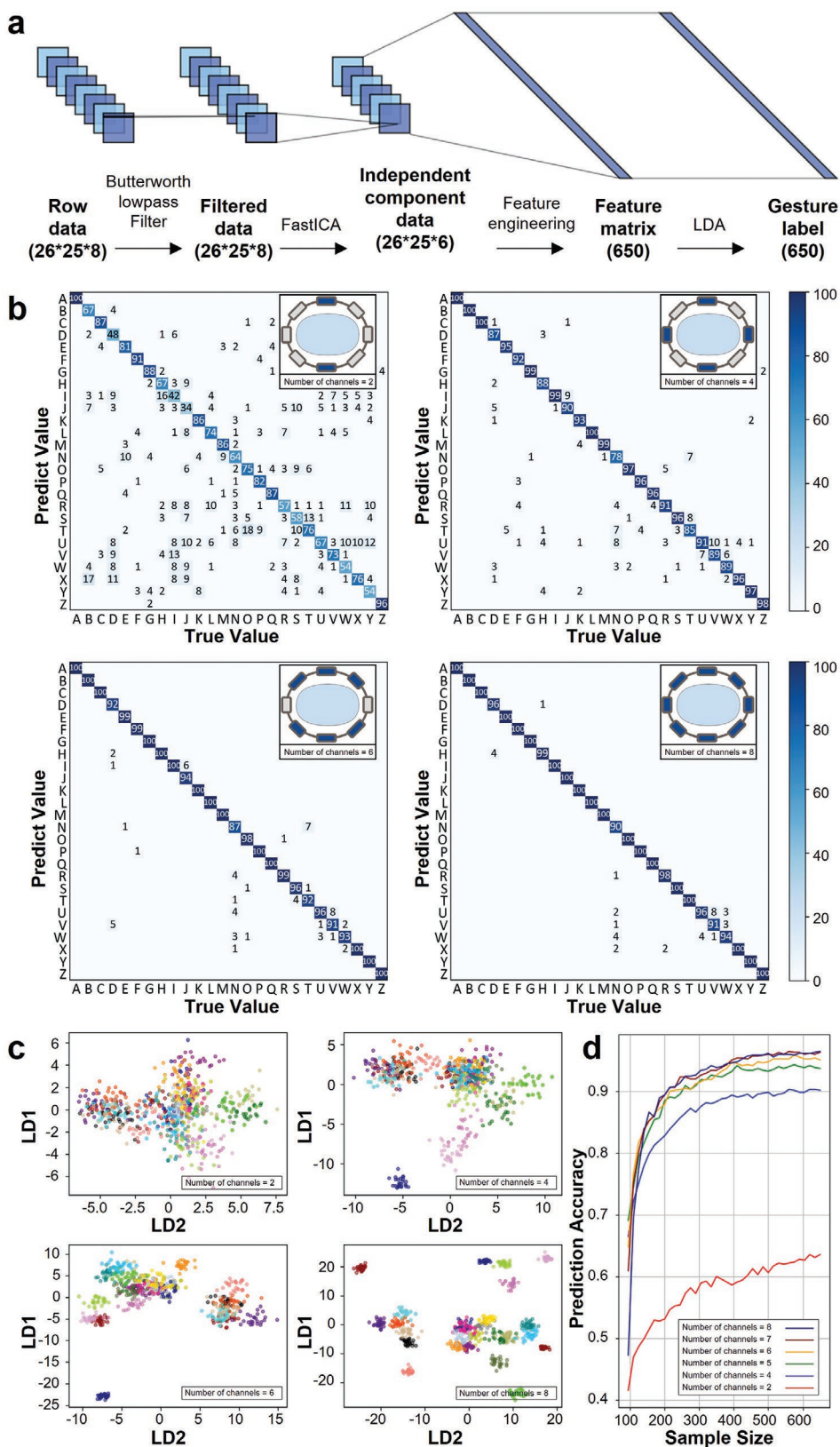


Figure 4. Processing methods and results of machine learning: a) Processing methods of machine learning. b) Confusion matrix of 26 letters in sign language when number of channels is 2 to 8. c) Cluster results of 26 letters in sign language when number of channels is 2 to 8. d) Prediction accuracy of model as sample size increases. When the number of channels was 8, the prediction accuracy of the model no longer improved significantly.

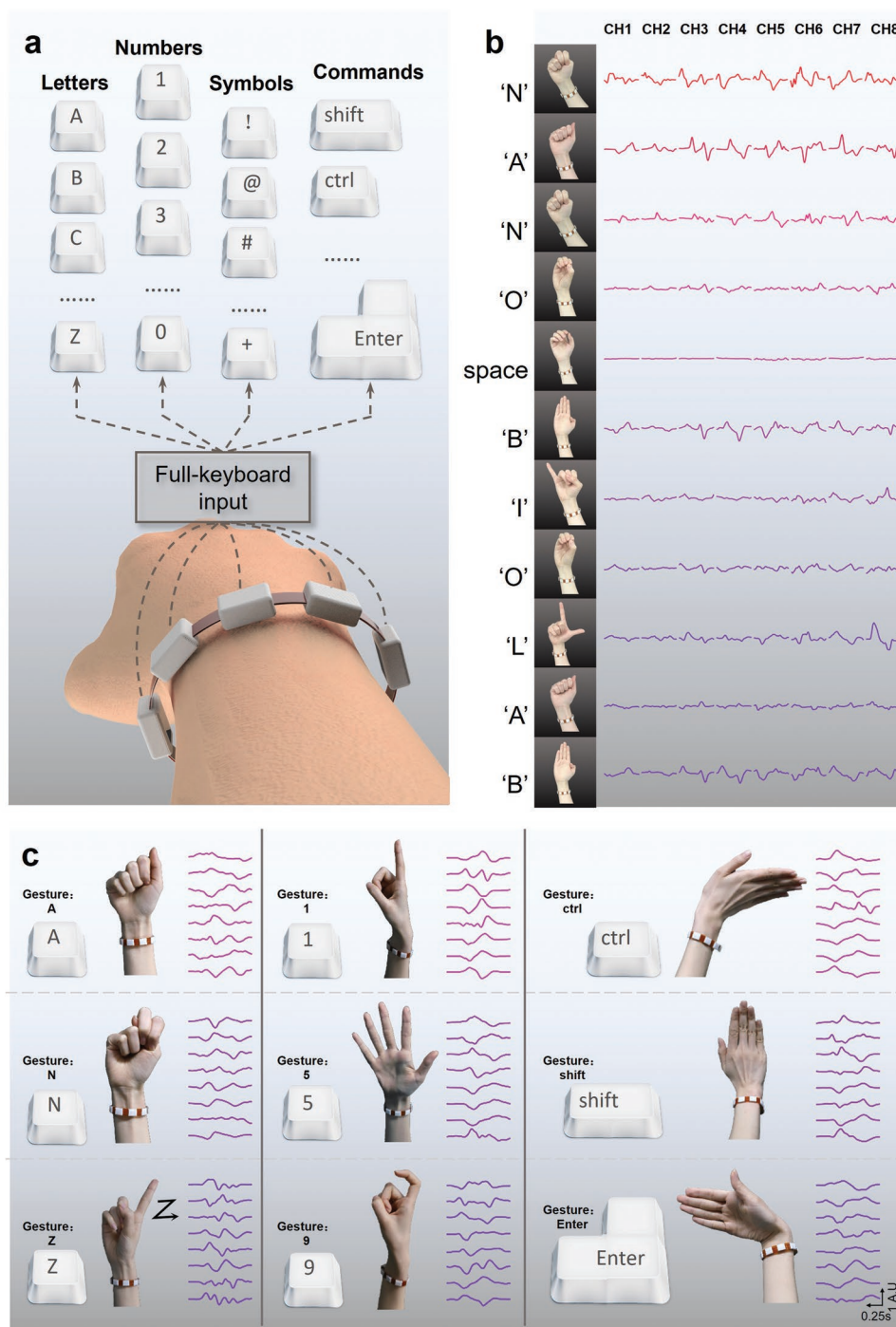


Figure 5. Specific implementation procedures of GRW: a) In addition to the international universal sign language gestures, specific numbers, symbols, and command symbols can be customized to design a complete wristband typing system. b) Real-time recognition signal of word “Nano biolab.” Computer detected letters and spaces individually, saved the input character, and then composed a complete sentence. c) Output results of some representative gestures of letters, numbers, and commands.

3. Conclusion

Our wristband was designed to solve three essential issues associated with HCI terminals. The first issue is portability.^[28–30] Consumers are more likely to accept products that resemble

existing wearable devices, such as watches and eyeglasses,^[31–34] instead of bulky mechanical devices. In this study, we integrated two types of sensors in a small box measuring 0.4 cm × 0.8 cm × 1 cm. The entire GRW can be worn easily on the wrist, and it does not affect the daily motion of the hands. The second

issue is the energy consumption of sensors.^[35–37] Existing sensors often require an excitation voltage as power supply. The active sensors employed in the GRW do not require excitation voltage.^[38–41] Therefore, this design will help GRW to reduce the energy consumption. Furthermore, because an additional power supply is not required, the size, weight, system complexity, and manufacturing costs of the GRW can be reduced significantly. The third issue associated with HCI terminals is accuracy.^[42–44] A full alphabet keyboard contains at least 61 letters. The accurate recognition of diverse signals from multiple sensor channels that reflect numerous types of gestures by a wristband, which allows information to be obtained from the skin surface, remains challenging in conventional data analysis and data processing methods. To improve the accuracy of the entire system, we designed a GRW using eight active sensors based on a hybrid generator comprising a TENG and a PENG. Combined with machine-learning technology, the GRW yielded accurate prediction results and achieved a high performance of 92.6%.

In addition to serving as an HCI terminal, the GRW can be used in healthcare, biomedical engineering, military, aerospace, and other fields. For example, the GRW can be utilized as a device that translates sign language based on gestures to language or sound. In particular, in certain silent environments, such as outer space or deep sea, or in other scenes where language communication is not possible, such as in combat or a conference, the GRW offers significant application potential. Owing to the development of the aforementioned technologies and specific usage scenarios, the GRW offers broad prospects in the fields of gesture command recognition, assistive devices for the disabled, and wearable electronics.

4. Experimental Section

Materials: PDMS was purchased from Dow Corning. Molds for the GRW were designed and printed using a 3D printer (Raize 3D) and PLA printing supplies. For wireless data acquisition and transmission, a commercial OpenBCI 8bit board (3IT EEG OBCI Kits) was used.

Fabrication: First, a layer of PDMS was cured onto the PLA mold. The main and curing agents (10:1 by weight) of the PDMS were mixed completely. Subsequently, the mixture was vacuumed for 30 min before it was poured into a container containing the previously prepared cured silicone. The FPCB was predesigned, whereas the PVDF and copper film were of the desired size. Subsequently, these materials were assembled piece by piece.

Characterization and Measurement: A linear motor (LinMot E1100) was utilized to continuously impart periodic mechanical traction to the GRW to maintain the operating cycle. A Keithley 6517 electrometer was used to measure the open-circuit voltage and short-circuit current of the GRW, and the data were obtained and recorded using an oscilloscope (LeCroy HDO6104). A wireless motion monitoring system based on an OpenBCI 8 bit board was used to record data from the GRW. A commercial mechanics sensor, SBT630, was used for a stress test. Standard weights from the Shanghai Weigh Instrument Factory were used in the calibration experiment of the sensor.

The experiments involving human subjects have been performed with the full, informed consent of the volunteers, who are also authors of the manuscript.

Supporting Information

Supporting Information is available from the Wiley Online Library or from the author.

Acknowledgements

This study was supported by the Strategic Priority Research Program of Chinese Academy of Sciences (XDA16021101), National Natural Science Foundation of China (61875015, T2125003, U20A20390, 11827803, 61922075), Beijing Natural Science Foundation (JQ20038), and the Fundamental Research Funds for the Central Universities for the support.

Conflict of Interest

The authors declare no conflict of interest.

Data Availability Statement

The data that support the findings of this study are available from the corresponding author upon reasonable request.

Keywords

gesture recognition, human–computer interaction, machine learning, triboelectric nanogenerator, virtual reality

Received: January 25, 2022

Revised: March 10, 2022

Published online:

- [1] F. Wen, Z. Zhang, T. He, C. Lee, *Nat. Commun.* **2021**, *12*, 5378.
- [2] W. Ding, A. Wang, C. Wu, H. Guo, Z. L. Wang, *Adv. Mater. Technol.* **2018**, *4*, 1800487.
- [3] X. Ji, T. Zhao, X. Zhao, X. Lu, T. Li, *Adv. Mater. Technol.* **2020**, *5*, 1900921.
- [4] X. Chou, J. Zhu, S. Qian, X. Niu, J. Qian, X. Hou, J. Mu, W. Geng, J. Cho, J. He, C. Xue, *Nano Energy* **2018**, *53*, 550.
- [5] G. Chen, X. Xiao, X. Zhao, T. Tat, M. Bick, J. Chen, *Chem. Rev.* **2022**, *122*, 3259.
- [6] G. Chen, X. Xiao, X. Zhao, T. Tat, M. Bick, J. Chen, *ACS Nano* **2021**, *15*, 18633.
- [7] Z. Lin, G. Zhang, X. Xiao, C. Au, Y. Zhou, C. Sun, Z. Zhou, R. Yan, E. Fan, S. Si, L. Weng, S. Mathur, J. Yang, J. Chen, *Adv. Funct. Mater.* **2022**, *32*, 2109430.
- [8] P. S. Das, A. Chhetry, P. Maharjan, M. S. Rasel, J. Y. Park, *Nano Res.* **2019**, *12*, 1789.
- [9] A. Moin, A. Zhou, A. Rahimi, A. Menon, S. Benatti, G. Alexandrov, S. Tamakloe, J. Ting, N. Yamamoto, Y. Khan, F. Burghardt, L. Benini, A. C. Arias, J. M. Rabaey, *Nat. Electron.* **2020**, *4*, 54.
- [10] M. Wang, Z. Yan, T. Wang, P. Cai, S. Gao, Y. Zeng, C. Wan, H. Wang, L. Pan, J. Yu, S. Pan, K. He, J. Lu, X. Chen, *Nat. Electron.* **2020**, *3*, 563.
- [11] X. Y. Wu, *Multimedia Tools Appl.* **2019**, *79*, 9193.
- [12] G. Li, H. Wu, G. Jiang, S. Xu, H. Liu, *IEEE Access* **2019**, *7*, 23713.
- [13] Y. Zou, P. Tan, B. Shi, H. Ouyang, D. Jiang, Z. Liu, H. Li, M. Yu, C. Wang, X. Qu, L. Zhao, Y. Fan, Z. L. Wang, Z. Li, *Nat. Commun.* **2019**, *10*, 2695.
- [14] G. Tian, W. Deng, Y. Gao, D. Xiong, C. Yan, X. He, T. Yang, L. Jin, X. Chu, H. Zhang, W. Yan, W. Yang, *Nano Energy* **2019**, *59*, 574.
- [15] Z. Zhou, K. Chen, X. Li, S. Zhang, Y. Wu, Y. Zhou, K. Meng, C. Sun, Q. He, W. Fan, E. Fan, Z. Lin, X. Tan, W. Deng, J. Yang, J. Chen, *Nat. Electron.* **2020**, *3*, 571.

- [16] M. H. Syu, Y. J. Guan, W. C. Lo, Y. K. Fuh, *Nano Energy* **2020**, *76*, 105029.
- [17] X. Pu, S. An, Q. Tang, H. Guo, C. Hu, *iScience* **2021**, *24*, 102027.
- [18] C. Wu, W. Ding, R. Liu, J. Wang, A. C. Wang, J. Wang, S. Li, Y. Zi, Z. L. Wang, *Mater. Today* **2018**, *21*, 216.
- [19] T. Jin, Z. Sun, L. Li, Q. Zhang, M. Zhu, Z. Zhang, G. Yuan, T. Chen, Y. Tian, X. Hou, C. Lee, *Nat. Commun.* **2020**, *11*, 5381.
- [20] G. Li, S. Liu, L. Wang, R. Zhu, *Sci. Rob.* **2020**, *5*, 49.
- [21] Q. He, Y. Wu, Z. Feng, C. Sun, W. Fan, Z. Zhou, K. Meng, E. Fan, J. Yang, *Nano Energy* **2019**, *59*, 689.
- [22] M. Khorsand, J. Tavakoli, H. Guan, Y. Tang, *Nano Energy* **2020**, *75*, 104993.
- [23] R. Ghosh, M. S. Song, J. Park, Y. Tchoe, P. Guha, W. Lee, Y. Lim, B. Kim, S.-W. Kim, M. Kim, G.-C. Yi, *Nano Energy* **2021**, *80*, 105537.
- [24] Y. Zou, A. Libanori, J. Xu, A. Nashalian, J. Chen, *Research* **2020**, *2020*, 7158953.
- [25] Q. Shi, B. Dong, T. He, Z. Sun, J. Zhu, Z. Zhang, C. Lee, *InfoMat* **2020**, *2*, 1131.
- [26] X. Ji, P. Fang, B. Xu, K. Xie, H. Yue, X. Luo, Z. Wang, X. Zhao, P. Shi, *Nano Lett.* **2020**, *20*, 4043.
- [27] J. H. Han, K. M. Bae, S. K. Hong, H. Park, J.-H. Kwak, H. S. Wang, D. J. Joe, J. H. Park, Y. H. Jung, S. Hur, C. D. Yoo, K. J. Lee, *Nano Energy* **2018**, *53*, 658.
- [28] Q. He, Y. Wu, Z. Feng, W. Fan, Z. Lin, C. Sun, Z. Zhou, K. Meng, W. Wu, J. Yang, *J. Mater. Chem. A* **2019**, *7*, 26804.
- [29] J. Kim, A. S. Campbell, B. E. de Avila, J. Wang, *Nat. Biotechnol.* **2019**, *37*, 389.
- [30] Y. Long, J. Li, F. Yang, J. Wang, X. Wang, *Adv. Sci.* **2021**, *8*, 2004023.
- [31] P. Prince, A. Hill, E. Pina Covarrubias, P. Doncaster, J. L. Snaddon, A. Rogers, *Sensors* **2019**, *19*, 553.
- [32] F.-R. Fan, Z.-Q. Tian, Z. L. Wang, *Nano Energy* **2012**, *1*, 328.
- [33] J. C. Yang, J. Mun, S. Y. Kwon, S. Park, Z. Bao, S. Park, *Adv. Mater.* **2019**, *31*, 1904765.
- [34] H. J. Yoon, D. M. Lee, Y. J. Kim, S. Jeon, J. H. Jung, S. S. Kwak, J. Kim, S. Kim, Y. Kim, S. W. Kim, *Adv. Funct. Mater.* **2021**, *31*, 2100649.
- [35] J. Yuan, R. Zhu, *Appl. Energy* **2020**, *271*, 115250.
- [36] L. Shu Fang, C. Y. Tsai, M. H. Xu, S. W. Wu, W. C. Lo, Y. H. Lu, Y. K. Fuh, *Nanotechnology* **2020**, *31*, 155502.
- [37] Y. Guo, M. Zhong, Z. Fang, P. Wan, G. Yu, *Nano Lett.* **2019**, *19*, 1143.
- [38] B. Sun, G. Zhou, K. Xu, Q. Yu, S. Duan, *ACS Mater. Lett.* **2020**, *2*, 1669.
- [39] Z. Zhou, L. Weng, T. Tat, A. Libanori, Z. Lin, L. Ge, J. Yang, J. Chen, *ACS Nano* **2020**, *14*, 14126.
- [40] H. Ouyang, D. Jiang, Y. Fan, Z. L. Wang, Z. Li, *Sci. Bull.* **2021**, *66*, 1709.
- [41] P. Tan, Q. Zheng, Y. Zou, B. Shi, D. Jiang, X. Qu, H. Ouyang, C. Zhao, Y. Cao, Y. Fan, Z. L. Wang, Z. Li, *Adv. Energy Mater.* **2019**, *9*, 1901875.
- [42] Y. LeCun, Y. Bengio, G. Hinton, *Nature* **2015**, *521*, 436.
- [43] S. Liu, J. Zhang, Y. Zhang, R. Zhu, *Nat. Commun.* **2020**, *11*, 5615.
- [44] Q. Shi, Z. Zhang, T. He, Z. Sun, B. Wang, Y. Feng, X. Shan, B. Salam, C. Lee, *Nat. Commun.* **2020**, *11*, 4609.